THE ASTROPHYSICAL JOURNAL, 344:637–644, 1989 September 15


# GRAVITATIONALLY LENSED IMAGES IN ABELL 370

SCOTT A. GROSSMAN AND RAMESH NARAYAN
Steward Observatory, University of Arizona
*Received 1988 December 16; accepted 1989 March 1*

## ABSTRACT

Several blue arclike images have been found in the galaxy cluster A370, some up to 1′ from the cluster center. We show that all the images can be explained by gravitational lensing of background galaxies, provided there is a significant amount of dark matter in the cluster. We use the observations to constrain the distribution of the dark matter. We find a mass-to-light ratio $M/L_B \sim 200$ and a projected half-density core radius of the dark matter $\lesssim 26''$ or $\lesssim 110$ kpc. The isodensity contours of the dark matter need to be elongated in the north-south direction with an axis ratio greater than about 4:3. The ratio is probably closer to 2:1. The longest arc has a measured redshift of 0.724, as opposed to the cluster redshift of 0.374. For the smaller arcs we require source redshifts $z_S \gtrsim 1.2$, with $z_S \sim 1.5$ giving the best fit. We suggest that the arcs are elongated and magnified images of a very numerous population of high-redshift blue galaxies identified by Tyson. Deep images of other galaxy clusters may reveal many more distorted images. An analysis similar to the one presented here may then lead to unique information on the morphology of the dark matter in these clusters.

*Subject headings:* dark matter — galaxies: clustering — gravitational lenses

## I. INTRODUCTION

The giant luminous arcs discovered in the galaxy clusters A370, Cl 2244−02, A963, and Cl 0500−24 (Soucail *et al.* 1987*a*; Lynds and Petrosian 1986; Lavery and Henry 1988; Giraud 1988) have been interpreted as gravitationally lensed images of background galaxies (Paczyński 1987). The redshift of the arc in A370 is greater than that of the lensing cluster (Soucail *et al.* 1988; Miller and Goodrich 1988; Lynds and Petrosian 1989), confirming the lensing hypothesis in this case. Grossman and Narayan (1988) studied the types and frequency of occurrence of gravitationally lensed images of galaxies lensed by clusters. They predicted that there should be several smaller arcs for each long arc observed (see also Blandford, Phinney, and Narayan 1986). Indeed, systems of smaller arcs have now been observed in the galaxy clusters A370 (Fort *et al.* 1988, hereafter F88) and A2218 (Pello-Descayre *et al.* 1988). We show here that such observations of multiple arcs in a single galaxy cluster provide useful information on the mass distribution in the cluster. In addition, galaxy clusters acting as "gravitational telescopes" may aid the identification and study of high-redshift galaxies.

Figure 1 is a representation of the central 140″ × 140″ of A370, showing the positions of the cluster galaxies and the arcs. The longest arc, A0, is the one originally discovered by Soucail *et al.* (1987*a*) and Lynds and Petrosian (1986). It has a radius of curvature of about 25″ and a length of 25″ (Soucail *et al.* 1987*b*). The eastern end of the arc is broken off and is bent with respect to the rest of the arc. The western part of the arc is about 0″.7 thick and the eastern part about 1″.5 thick. The smaller arcs A1–A6 have lengths of 3″, 4″, 3″, 2″.5, 9″.3, and 6″.5, respectively (F88). In addition, there are three images B1, B2, B3 near the center of the cluster which may also be lensed. All the images, A0–A6, B1–B3, are blue in color, indicating that the corresponding sources may be spiral galaxies at redshifts, $z_S \approx 1$. (Because A6 is in a crowded part of the field, it may conceivably be two images or even a chain of very blue cluster members.) The most noteworthy feature of the arcs is that several of them, especially A5 and A6, are located much farther from the cluster center than the dominant arc, A0. This raises an important question: can the elongated outer arcs be produced by gravitational lensing, and if they are, what constraints can be set on the cluster mass distribution in A370?

We address this question in this paper. We show that gravitational lensing can indeed account for the positions and lengths of the observed arcs without having to resort to any extreme or peculiar cluster mass distribution. In § II we discuss the model of the mass distribution we use to describe the cluster. The dark matter is parametrized by its core radius and ellipticity. In § III we present our best cluster model. This model is able to reproduce the main qualitative features of the observations, with reasonable quantitative agreement. In § IV we consider the uniqueness of our model and discuss what constraints we can place on the core radius and ellipticity of the cluster and on the redshifts of the background galaxies. In § V we discuss the implications of our results and suggest future observations. Models of A370 have previously been constructed and simulations of A0 performed by Hammer (1987), Soucail *et al.* (1987*b*), and Narasimha and Chitre (1988).

## II. THE MODEL

We model the surface density of the cluster as the sum of two components: a continuous, smooth component representing the dark matter, and a clumpy component representing the luminous mass associated with individual galaxies. The smooth component dominates the mass of the cluster and is parametrized by a core radius, $r_c$, and an ellipticity, $\epsilon$. We assume the following form,

$$\Sigma(\boldsymbol{r}_I) = \frac{\sigma^2/2GD_{OL}r_c}{[1 + (1 + \epsilon)(x/r_c)^2 + (1 - \epsilon)(y/r_c)^2]^{1/2}}, \qquad (1)$$

which is an elliptical generalization of a nonsingular isothermal sphere. The position vector $\boldsymbol{r}_I \equiv (x, y)$ represents the angular position in the lens/image plane, measured with respect to the center of the cluster; the axes are chosen to be

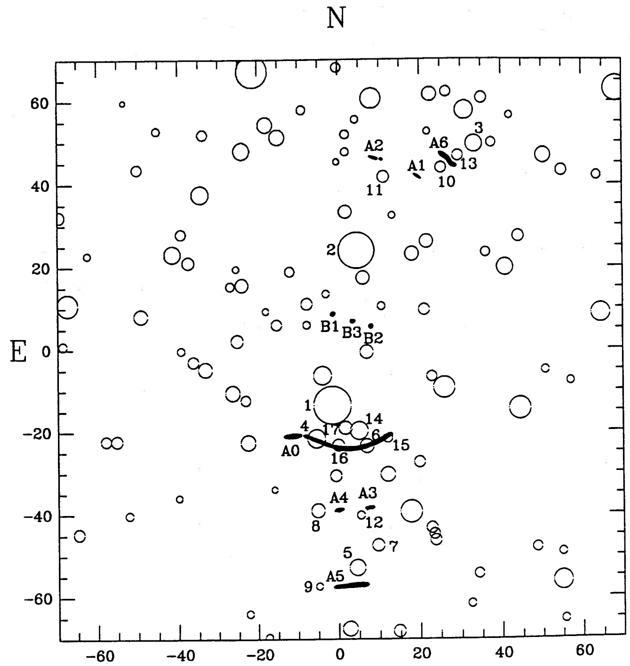


FIG. 1.—Shows the central 140″ × 140″ of A370, with the arcs A0–A6 accurately sketched in. The objects B1–B3 may also be gravitationally lensed images. The galaxies of A370, plotted as open circles, are taken from BOW. Individual galaxies that we included in the lensing calculation (Table 1) are labeled. The scale is in arcseconds.

parallel to the principal axes of the elliptical surface density. The quantity $D_{OL}$ is the observer-lens angular diameter distance, and $\sigma$ is the one-dimensional velocity dispersion of the cluster. The scaling of $\Sigma$ with $\sigma^2$ strictly applies only to a spherically symmetric cluster. In the more general case there is an additional factor that depends on the magnitude of $\epsilon$, on the unknown extent of the cluster along the line of sight, and on the shape of the velocity dispersion ellipsoid; however, this factor is expected to be $\sim 1$ for reasonable models. We set $\sigma = 1367$ km s$^{-1}$, the observed line-of-sight velocity dispersion of A370 (Henry and Lavery 1987). The redshift of the lensing cluster is $z_L = 0.374$. These values of $\sigma$ and $z_L$ are confirmed by Mellier *et al.* (1988). Furthermore, they demonstrate that the galaxy counts are asymptotically isothermal, giving additional support to our choice of the form of $\Sigma(\boldsymbol{r}_I)$.

Figure 1 shows that each of the smaller arcs in A370 is near one or more foreground galaxies, and one might suspect that these particular galaxies significantly affect the shapes of these images. Also, the two massive cD galaxies near the center of the cluster probably have a significant influence over a wide region around them. Therefore, we superpose upon the smooth mass distribution the surface densities of selected galaxies that we suspect may be important. We model the surface densities of the galaxies by singular truncated isothermal spheres,

$$\Sigma_g(r) = \frac{\sigma_g{}^2}{2GD_{OL}r}, \quad D_{OL}r \le R_{\rm outer}, \tag{2}$$

where $r$ is the angular radius from the center of the galaxy and $\sigma_g$ the one-dimensional velocity dispersion. We take the outer radius to be $R_{\rm outer} = 14.0\ (L_B/L_*)^{1/2}$ kpc $= 14.0\ (\sigma_g/\sigma_*)^2$ kpc (see Grossman and Narayan 1988), where $L_* = 1.5 \times 10^{10}\ L_\odot$ characterizes the galaxy luminosity at the bend in the Schechter luminosity function (Schechter 1976; Mihalas and Binney 1981). We take $\sigma_* = 220$ km s$^{-1}$ (Fall 1981).

To determine $R_{\rm outer}$ and $\sigma_g$ for the galaxies, we use the photometry of Butcher, Oemler, and Wells (1983, herafter BOW) and the classifications of MacLaren, Ellis, and Couch (1988, hereafter MEC). BOW give $J$ magnitudes, from which $B$ magnitudes can be calculated from the relationship $B = J + 0.23$ $(B-V)$ (see MEC). We take $B-V \approx 1.4$ as a characteristic color of galaxies at $z_L = 0.374$ (Pence 1976). By applying the appropriate $K$-corrections based on galaxy type (Pence 1976) and calculating the luminosity distance of the cluster for an $\Omega = 1$, $H_0 = 75$ km s$^{-1}$ Mpc$^{-1}$ universe, we calculate the absolute $B$ magnitude, and hence the ratio $L_B/L_*$, given that $M_B{}^* = -19.7$ (Schechter 1976). From this we determine $R_{\rm outer}$ and $\sigma_g$. We follow a different procedure for the two cD galaxies, since they do not follow the Schechter luminosity function. We arbitrarily choose $R_{\rm outer} = 46$ kpc and $\sigma_g = 400$ km s$^{-1}$ for these galaxies, which are reasonable estimates. We also include in our list of galaxies all those used by Hammer (1987) in his simulation of A0, not all of which are in BOW. For Hammer's galaxies 63, c, g, and h we estimate the positions and radii from Figure 2 of his paper. The list of galaxies that we include in the calculations is given in Table 1, along with the relevant parameters. The galaxy coordinates are found by translating the origin of the BOW coordinates to (766, 830), coinciding with position $C'$ of F88. The coordinates are rotated by 180° and scaled to units of arcseconds. In order to be consistent with the measured $\sigma$, we reduce the mass of the smooth component of the cluster so that the total mass within a radius of 60″, including the individual galaxies, remains unchanged. This correction is fairly small ($\approx 5\%$).

For a point source at position $\boldsymbol{r}_S$, the locations $\boldsymbol{r}_I$ of the lensed images are found by solving the implicit equation,

$$\boldsymbol{r}_S = \boldsymbol{r}_I - \frac{D_{LS}}{D_{OL}D_{OS}} \frac{2}{c^2} \nabla\phi(\boldsymbol{r}_I), \tag{3}$$

where $\phi$ is the two-dimensional Newtonian gravitational potential associated with the lens and $D_{OS}$ and $D_{LS}$ are the observer-source and lens-source angular diameter distances. The potential is obtained by solving the two-dimensional Poisson's equation,

$$\nabla^2\phi(\boldsymbol{r}_I) = 4\pi G\Sigma(\boldsymbol{r}_I). \tag{4}$$

For an extended source such as a background galaxy, $\boldsymbol{r}_S$ ranges over an area in the source plane, which maps to one or more bounded areas in the image plane. These areas represent the images. We solve equations (3) and (4) with a computer algorithm we have developed that handles an arbitrary surface density model of the lens. The code also calculates the set of points on which the determinant of the Jacobian $|\partial\boldsymbol{r}_S/\partial\boldsymbol{r}_I|$ vanishes. These points define *critical lines* in the image plane and *caustics* in the source plane. Images are infinitely magnified on critical lines, and merging images form or disappear in pairs across them. Caustics and critical lines are useful tools to aid one's understanding of the lensing properties of a mass distribution (Grossman and Narayan 1988; Narayan and Grossman 1988).

## III. THE BEST MODEL OF A370

In attempting to model the surface density of A370, we work under the assumption that five background galaxies are required to simulate the observations. We assume that the arcs

TABLE 1

PARAMETERS OF LENSING GALAXIES

| No. | BOW No. | $x$ (arcsec)[a] | $y$ (arcsec)[a] | Type[b] | $m_B$[c] | $M_B$[c] | $L_B/L_*$[d] | $\sigma$ (km s$^{-1}$) | $R_{\rm outer}$ (kpc) | $M/M_\odot \times 10^{-11}$ |
|---|---|---|---|---|---|---|---|---|---|---|
| 1 ......... | 9 | −1.5 | −13.5 | E/SO | 21.05 | −21.5 | 5.2 | 400[e] | 46.0 | 53 |
| 2 ......... | 10 | 4.5 | 24.0 | E/SO | 21.26 | −21.3 | 4.4 | 400[e] | 46.0 | 53 |
| 3 ......... | 34 | 33.3 | 49.5 | E/SO | 21.97 | −20.6 | 2.3 | 271 | 21.2 | 11 |
| 4 ......... | 49 | −5.4 | −21.6 | E/SO | 21.85 | −20.7 | 2.5 | 306 | 22.1 | 15 |
| 5 ......... | 71 | 4.5 | −52.8 | E/SO[f] | 22.12 | −20.4 | 1.9 | 258 | 19.2 | 9.3 |
| 6 ......... | 91 | 6.9 | −23.4 | E/SO[f] | 22.38 | −20.2 | 1.5 | 243 | 17.1 | 7.4 |
| 7 ......... | 95 | 9.6 | −47.4 | E/SO[f] | 22.69 | −19.9 | 1.2 | 230 | 15.3 | 5.9 |
| 8 ......... | 181 | −5.1 | −39.0 | Scd[f] | 22.41 | −19.3 | 0.69 | 201 | 11.6 | 3.4 |
| 9 ......... | 216 | −4.8 | −57.3 | E/SO[f] | 23.89 | −18.7 | 0.39 | 174 | 8.8 | 1.9 |
| 10 ......... | 256 | 25.2 | 43.8 | Scd | 23.02 | −18.7 | 0.40 | 175 | 8.9 | 2.0 |
| 11 ......... | 372 | 11.1 | 41.7 | Scd | 22.84 | −18.9 | 0.48 | 183 | 9.7 | 2.3 |
| 12 ......... | 393 | 5.4 | −40.2 | Scd[f] | 23.60 | −18.1 | 0.23 | 152 | 6.7 | 1.1 |
| 13 ......... | [g] | 29.3 | 46.7 | Scd[f] | 23.02 | −18.7 | 0.40 | 175 | 8.9 | 2.0 |
| 14 ......... | [h] | 5.0 | −19.7 | E/SO[f] | 22.3 | −20.3 | 1.7 | 251 | 18.0 | 8.3 |
| 15 ......... | [h] | 12.0 | −21.5 | E/SO[f] | 23.9 | −18.7 | 0.41 | 176 | 9.0 | 2.0 |
| 16 ......... | [h] | 0.0 | −23.2 | E/SO[f] | 23.3 | −19.3 | 0.72 | 203 | 12.0 | 3.6 |
| 17 ......... | [h] | 1.7 | −19.0 | E/SO[f] | 23.1 | −19.5 | 0.86 | 212 | 13.0 | 4.3 |

[a] Coordinates centered on BOW coordinates (766,830), corresponding to position C′ in F88. This coordinate system is rotated 180° with respect to BOW coordinates.
[b] Taken from MEC when available.
[c] The uncertainty on $m_B$ is estimated to be $\pm 0.07$. The uncertainty on $M_B$ is estimated to be $\pm 0.2$.
[d] $L_* = 1.5 \times 10^{10}\,L_\odot$.
[e] These are cD galaxies, whose velocity dispersions are larger than the Faber-Jackson law implies.
[f] Guess of galaxy type based on galaxy size, shape, and color.
[g] Assume properties the same as BOW No. 256.
[h] Galaxies included in calculations of Hammer (1987). Sizes are estimated from his figure. Galaxies 14–17 correspond to his labels 63, c, g, and h, respectively.

A0, A5, and A6 are each produced by one galaxy, while the pairs A1–A2 and A3–A4 each arise from a single galaxy. We do not attempt to fit the images B1, B2, B3. The two cD galaxies in A370 are separated roughly in a north-south direction. Also, the arcs tend to be preferentially located along a similar axis. Both these facts suggest that the dominant dark matter in the cluster may be elongated in the north-south direction. Keeping this in mind we consider only models in which the principal $x$ and $y$ axes of equation (1) are oriented parallel to right ascension and declination, respectively. North-south elongation then corresponds to positive $\epsilon$. We choose the center of the cluster to coincide with position $C'$ of F88, which is approximately midway between the two cD galaxies. For the arc A0, we use the observed redshift $z_S = 0.724$ (Soucail *et al.* 1988; Miller and Goodrich 1988; Lynds and Petrosian 1989). We place the other source galaxies at $z_S = 1.2$, which is consistent with the observed colors, given the uncertainties in galaxy $K$-corrections (F88; Coleman, Wu, and Weedman 1980).

After trying several sets of parameters, we conclude that a model with $\epsilon = 0.6$ and $r_c = 10''$ (corresponding to a linear dimension of 42 kpc) comes closest to reproducing the important features of the observed arcs. Figure 2 shows the results and Table 2 gives the positions, redshifts, and angular sizes of the background galaxies. The small squares in Figure 2 are the positions of the lensing galaxies that are included in the calculations (see Table 1). The radii of the background galaxies are chosen to be compatible with the sizes of the caustics responsible for the corresponding arcs. The consequences of varying the parameters, $\epsilon$ and $r_c$, of the model will be discussed in the next section.

TABLE 2

PARAMETERS OF SOURCE GALAXIES

| $x_s$ (arcsec) | $y_s$ (arcsec) | $z_s$ | Scale (kpc) | Radius[a] (arcsec) | Images |
|---|---|---|---|---|---|
| 0.20 ........... | −11.10 | 0.724 | 3.0[b] | 0.56[b] | A0 |
| 2.28 ........... | 21.20 | 1.2 | 1.5 | 0.26 | A1–A2 |
| 0.15 ........... | −18.80 | 1.2 | 0.85 | 0.15 | A3–A4 |
| 1.45 ........... | −32.10 | 1.2 | 2.0 | 0.35 | A5 |
| 9.60 ........... | −28.00 | 1.2 | 3.0 | 0.52 | A6 |

[a] Assuming galaxies have exponential profiles. $H_0 = 75$ km s$^{-1}$ Mpc$^{-1}$, $\Omega = 1$.
[b] $\epsilon = 0.8$, position angle = 120°. All other source galaxies are circular.

Figure 2*a* shows the A0 simulation and the associated caustics and critical lines, assuming $z_S = 0.724$. We see that the cluster model reproduces A0 quite well. The western piece of the arc is 24″.9 long, several arcseconds longer than the observed length. The average width is 1″.6, about twice the observed width. The eastern end of the arc is broken across a critical line and is bent with respect to the rest of the arc. This bend is present in the observations and our ability to reproduce it represents an improvement over previous simulations of A0 (Soucail *et al.* 1987*b*; Hammer 1987; Narasimha and Chitre 1988). The eastern piece is 4″.8 long and 2″.1 wide. The increased width of this piece is consistent with the observations. We find that in our simulation the source galaxy has to be elliptical in order to produce an arc with the right shape. We require an eccentricity of 0.42 ($\epsilon = 0.8$) at a position angle of 120°.

Figure 2*b* shows the remaining images A1–A6 and their associated critical lines, assuming $z_S = 1.2$. Of particular interest is the dramatic change in the structure of the caustics and critical lines when the source plane is moved to the higher redshift of $z_S = 1.2$. The critical lines increase in angular scale and some galaxy critical lines merge with the overall cluster critical line. The larger scale of the critical lines leads to longer arcs and the possibility of producing arcs farther from the center. In some regions, such as the A3–A4 region, critical line mergers greatly increase the complexity of the image behavior.

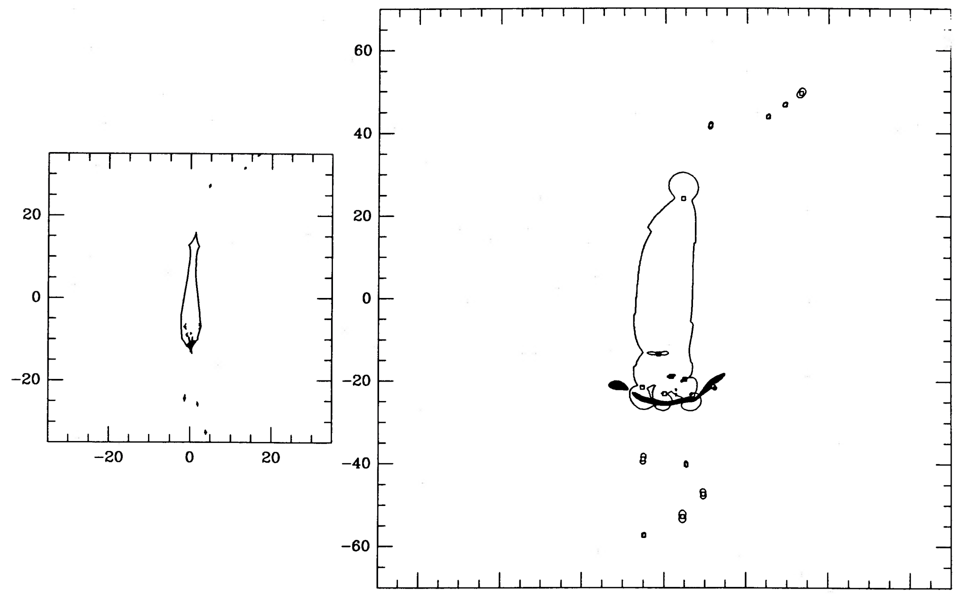


FIG. 2*a*

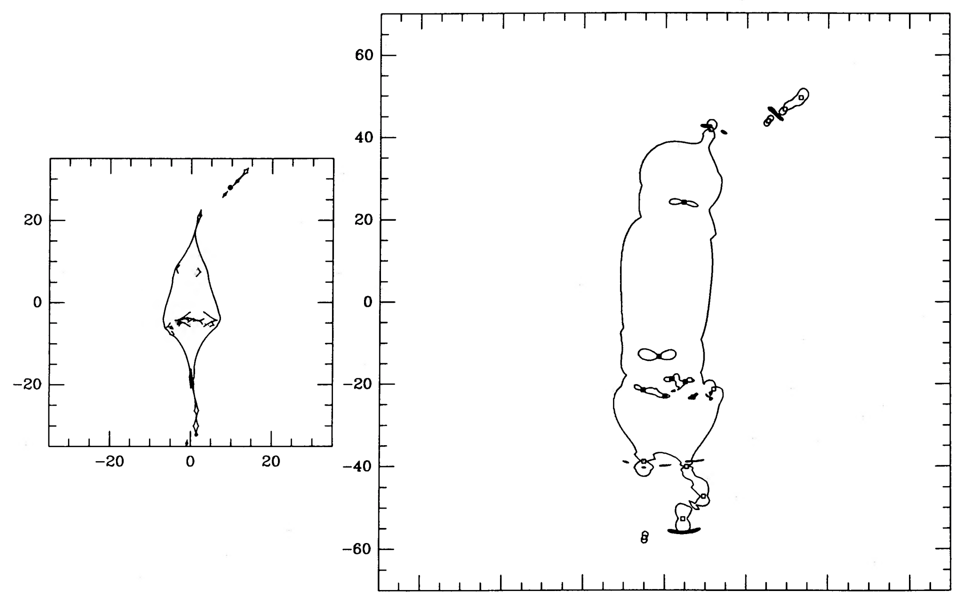


FIG. 2*b*

FIG. 2.—Shows our best simulation of the A370 arcs, for $\epsilon = 0.6$, $r_c = 10''$. The left-hand panels show the source planes with the source galaxies in their true positions. The lines are *caustics*. The right-hand panels are the image planes. The small boxes represent the galaxies included in the lensing calculation (labeled in Fig. 1). The lines are *critical lines*. (*a*) Our best simulation of the A0 arc. The source plane is at $z_s = 0.724$, the observed redshift of A0. (*b*) Our best simulation of A1–A6. The source plane is at a redshift of $z_s = 1.2$, consistent with the observed colors of the images if they are normal spiral galaxies. Images A1 and A2 arise from the same source galaxy, as do images A3 and A4. The arcs A5 and A6 each arise from an independent source galaxy.

In simulating the arcs A1–A6, we restrict ourselves to circular background galaxies and vary only their positions and radii.

A5 is second only to A0 in length, and because its distance from the cluster center is about twice that of A0, it is potentially the most difficult to understand. The simulated A5 in Figure 2*b* is 8″.3 long, compared to the observed length of 9″.3. We find that galaxy 5 plays an important role in the presence of this arc at such a large distance from the cluster center, but the dark matter in the cluster also contributes significantly to the length of the arc. The source galaxy is located on a cusp caustic. The simulation of A5 is robust in the sense that the source galaxy can be moved by a significant fraction of its radius without affecting the image. We consider that the length of A5 in the simulation is in satisfactory agreement with the observations. However, the shape and position are not very good. The observed arc is fairly straight and is shifted about 4″ east of the calculated position. We have not neglected any important galaxies in the vicinity of A5, so we suggest that the straightness of the observed arc may indicate the presence of nonluminous mass south of it.

The simulated A6 arc is 4".8 long, which should be compared to its true length of 6".5. Lensing galaxies 10 and 13 are primarily responsible for producing an arc at such a large radius and once again the dark matter contributes to the length of the arc. The presence of galaxies of comparable mass on either side of the arc is the reason for its straight shape. This arc is again fairly robust—the source galaxy can be moved by approximately its own radius without destroying the arclike appearance of the image.

The simulated A1 and A2 arcs are images of the same background galaxy and have lengths of 1".6 and 2".8, compared to the measured lengths of 3" and 4", respectively. The calculated separation is not as large as the observed separation, which is a little hard to explain since there are no lensing galaxies in the immediate vicinity that we have ignored. It might be possible to improve the agreement by associating more dark matter directly with the galaxies rather than with the cluster.

The simulated A3–A4 arcs and accompanying images are quite complex. We obtain lengths of 4".2 and 2".8 for A3 and A4 (using a single background galaxy), compared to the observed lengths of 3" and 2".5. The merging of galaxy critical lines with the cluster critical lines increases the complexity of caustics in such a way that additional images are always obtained when the A3–A4 images are in the right positions. The longest extra image, on the left, is 1".3. It is interesting that a small image does appear to be present at this position in the observations of F88 (see their Fig. 1).

The A1–A2 and A3–A4 arcs are not robust. The source galaxies must be positioned very carefully with respect to the fold caustics, the details of which are sensitive to small changes in the local mass distribution.

## IV. CONSTRAINTS ON LENS PARAMETERS AND SOURCE REDSHIFTS

We consider now how the lengths of the longer arcs, A0, A5, and A6, depend on the ellipticity, $\epsilon$, and core radius, $r_c$, of the dark matter in A370. We do not include A1–A4 in this discussion because these arcs are shorter and depend very sensitively on details of the local mass distribution, in particular the positions and sizes of nearby galaxies.

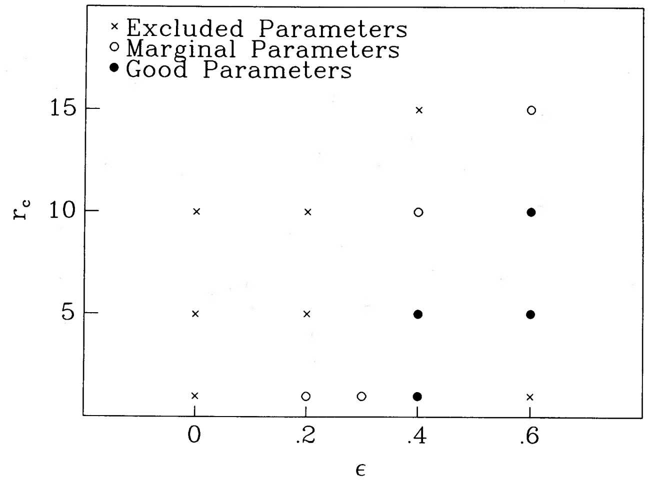


FIG. 3.—Summarized results of various models tested (see Table 3). Each model consists of a choice of core radius, $r_c$, and ellipticity, $\epsilon$. Models that pass our acceptability tests on all counts are represented by the symbol ●. Marginal models, which almost meet our criteria, are represented by ○. Models that do not come close to our criteria are represented by ×.

Table 3 and Figure 3 show the results for a grid of the model parameters, $r_c$ and $\epsilon$. In all cases we assume that the source galaxy of A0 is at $z_S = 0.724$ and those of A5, A6 are at $z_S = 1.2$. We consider a model acceptable if it produces an A0 west arc longer than 16".6 and an A5 arc longer than 7".4 (80% of the observed lengths). With this criterion, only four models, including the "best model" of § III, are acceptable. In addition, a number of other models are marginal in the sense that they miss our criterion by only a small amount. Models with low values of $\epsilon$ produce A0 arcs which are not only too short, but also highly distorted. Figure 4 shows a simulation of A0 with $\epsilon = 0$, $r_c = 10''$, which is an example of a typical "bad arc."

Based on the results given in Table 3 and Figure 3, we can state that $\epsilon$ has to be $\gtrsim 0.3$ for an acceptable fit. This corresponds to models with major-to-minor axis ratios greater than 4:3. Our best model has $\epsilon = 0.6$, corresponding to an axis ratio of 2:1. If we take $\epsilon = 0.6$ as a reasonable upper limit to the ellipticity, then we also deduce that $r_c$ needs to be $\lesssim 15''$.

Almost every model we have considered fails to produce a long enough A6 arc, and, indeed most of them are a little deficient even in the case of the A5 arc. This might suggest that the assumed redshifts of these sources are incorrect. Table 4 shows the effect on A5 and A6 of assuming different values of

TABLE 3

ARC LENGTHS FOR MODELS WITH VARIOUS ELLIPTICIES AND CORE RADII[a]

| $\epsilon$ | $r_c$ | AO (west) | AO (east) | A5 | A6 |
|---|---|---|---|---|---|
| 0.0 ........ | 1 | 28.6 | 7.1 | 6.3 | 4.9 |
| 0.2 ........ | 1 | 29.3 | 8.3 | 7.1 | 5.3 |
| 0.3 ........ | 1 | 25.5 | 10.3 | 7.2 | 5.4 |
| 0.4 ........ | 1 | 27.5 | 8.9 | 8.7 | 5.9 |
| 0.6 ........ | 1 | 12.6 | 4.4 | 9.9 | 6.5 |
| 0.0 ........ | 5 | ~19.0 | 5.3 | 5.8 | 4.3 |
| 0.2 ........ | 5 | ~26.0 | 4.4 | 6.1 | 4.7 |
| 0.4 ........ | 5 | 26.6 | 4.6 | 7.4 | 5.0 |
| 0.6 ........ | 5 | 24.2 | 7.0 | 9.5 | 5.6 |
| 0.0 ........ | 10 | 14.4 | 3.5 | 5.6 | 4.2 |
| 0.2 ........ | 10 | ~17.0 | 4.7 | 6.0 | 4.1 |
| 0.4 ........ | 10 | 20.8 | 3.4 | 6.7 | 4.6 |
| 0.6 ........ | 10 | 24.9 | 4.8 | 8.3 | 4.8 |
| 0.4 ........ | 15 | 14.5 | 3.8 | 6.0 | 3.9 |
| 0.6 ........ | 15 | 16.2 | 4.4 | 7.5 | 4.2 |
| Observed................ | | 20.7 | 4.3 | 9.3 | 6.5 |
| requirements ........... | | >16.6 | | >7.4 | |

[a] Arc lengths and core radii are measured in arcseconds.

TABLE 4

LENGTHS[a] OF A5 AND A6 AS FUNCTIONS OF SOURCE REDSHIFTS FOR $\epsilon = 0.6$, $r_c = 10''$

| $z_s$ | A5 | A6 |
|---|---|---|
| 1.0......... | 7.1 | 3.7 |
| 1.2......... | 8.3 | 4.8 |
| 1.4......... | 8.9 | 5.6 |
| 1.6......... | 10.0 | 6.2 |
| 1.8......... | 10.5 | 6.9 |
| 2.0......... | 11.0 | 7.5 |

[a] Lengths in arcseconds.

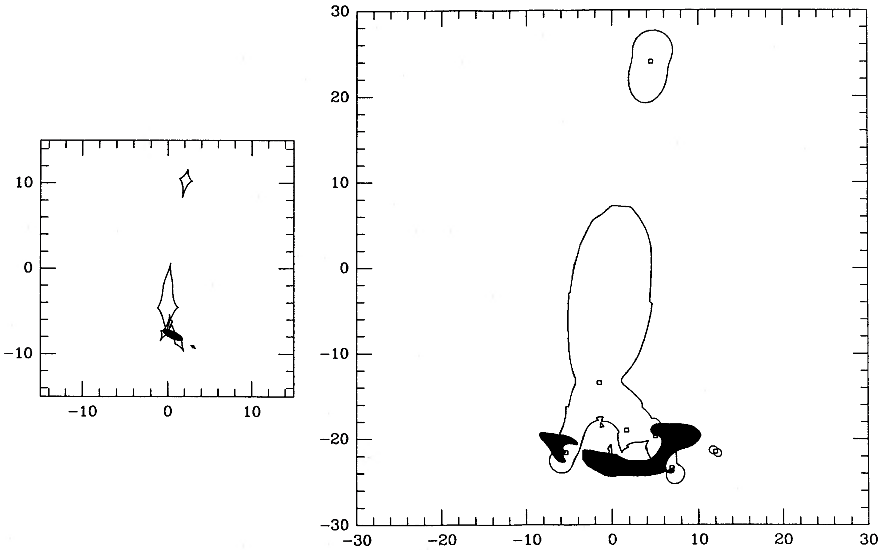


FIG. 4.—An example of a typical "bad arc." This is a simulation of A0 with a lens model corresponding to $\epsilon = 0$, $r_c = 10''$ and the source plane at redshift $z_s = 0.724$. Models with nearly circularly symmetric distributions of dark matter yield arcs which are both too short and too distorted.

$z_S$, keeping $\epsilon$ and $r_c$ fixed at 0.6 and 10″ (the best model). We see that with $z_S \gtrsim 1.5$, a much better fit is possible. Such a high redshift is apparently not consistent with the observed blue colors of the arcs if the background sources are unevolved normal spiral galaxies (Coleman, Wu, and Weedman 1980), but it may be consistent when evolutionary effects are considered. Indeed, Tyson (1988) is finding increasing evidence for a population of distant very blue galaxies, most of which are apparently at high redshifts $z_S > 2$.

## V. DISCUSSION AND CONCLUSIONS

We have demonstrated that all the arcs in A370 can be understood as gravitationally lensed images of background galaxies. The presence of arcs longer than a few arcseconds at radii well beyond A0 does not rule out the lensing hypothesis for these images as one might have at first imagined, but their presence (as well as the structure of A0) does require that the dark matter in the lens have an elliptical distribution. We find that models in which the surface density distribution has its major axis approximately parallel to the line connecting the two cD galaxies come closest to fitting the observations.

Our best model for A370 has most of the mass in a nonluminous form, modeled by the elliptical "isothermal" distribution of equation (1). If we consider the elliptical isodensity contour that passes through A0, we find a total interior mass of $6.2 \times 10^{13}\ M_\odot$, while the interior blue luminosity (including all the BOW galaxies) is only about $3.3 \times 10^{11}\ L$. This corresponds to a rather large mass-to-light ratio of $M/L_B \sim 190$. Soucail *et al.* (1988) find $M/L_R \sim 100$, which is consistent with our estimate of $M/L_B$. A similar exercise for the outer A5 arc leads to $M/L_B \sim 210$. Mellier *et al.* (1988) find $M/L_B = 165 \pm 45$, again in good agreement with our results. The two cD galaxies, which dominate the luminous mass in the center of the cluster, have $M/L_B \sim 65$ (Table 1), and the X-ray emitting intracluster gas probably accounts for about 30% of the mass of the cluster (Sarazin 1988). The remaining mass is probably dark matter, distributed smoothly across the cluster. This matter accounts for at least $M/L_B \sim 75$. (Note that unlike the value of Soucail *et al.*, our mass-to-light ratio is not virial independent, since we derive the mass of the cluster from the observed velocity dispersion.)

One of the important results of this paper is that we are able to go beyond the simple $M/L$ ratio and actually to set limits on the parameters describing the dark matter distribution in A370. The results are shown in Table 3 and Figure 3. We find that the ellipticity parameter, $\epsilon$, has to be $\gtrsim 0.3$, which means that the axis ratio must be greater than about 4:3. We have demonstrated that superposing a circularly symmetric dark matter distribution on the luminous matter, i.e., setting $\epsilon = 0$, does not come close to fitting the observations, as shown in Figure 4. We have also tried models with two independent circularly symmetric mass distributions centered on the two cD galaxies. Such models are a little better, but still fail under the criteria employed in § IV.

The second constraint we obtain is that $r_c \lesssim 15''$, with the preferred value being $r_c \sim 10''$ (our best model). At the distance of A370, this corresponds to a linear scale of 62 kpc. The radius at which the surface density falls to half its central value is $r_{1/2} = 3^{1/2} r_c$ (for a circular lens), and the constraint on this is $r_{1/2} \lesssim 26''$ or $\lesssim 108$ kpc, in good agreement with the value of 107 kpc derived by Mellier *et al.* (1988) (after correcting for different values of $H_0$; see also Thompson 1986). The X-ray core radius is $102^{+54}_{-36}{}''$ (Lea and Henry 1988), which is much larger than our value. However, a single core radius may not be meaningful for many clusters, since they show substructure and are not virialized (Fitchett 1988). In particular, A370, with two cD galaxies, shows evidence for substructure in its core, and this may account in part for the discrepancy between the X-ray core radius and our upper limit.

Although we have restricted ourselves to a redshift of 1.2 for the background sources of arcs A1–A6, our calculations suggest a somewhat higher redshift, say $\sim 1.5$, particularly for A5 and A6. The observed colors of these arcs are probably not consistent with normal spiral galaxies at such a large redshift, but it is conceivable that, as a result of evolutionary effects, galaxies at earlier epochs differ significantly from galaxies today. Indeed, Tyson (1988) finds a large population of distant

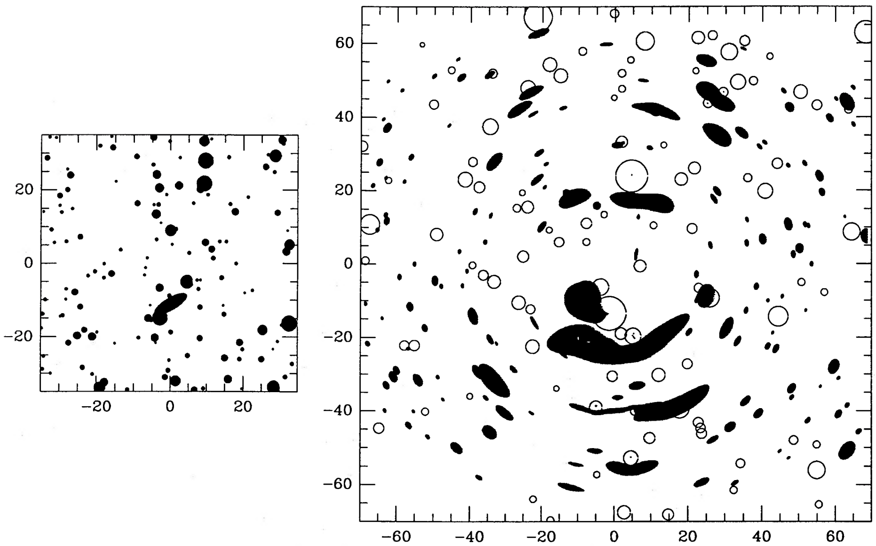

FIG. 5.—A simulation of what A370 might look like if a population of faint background source galaxies could be seen. The simulated source plane is populated with galaxies with a number density equivalent to that observed by Tyson (1988) down to $B_J = 27$. Note the tangential stretching of the images into small arcs, particularly along the major-axis of the dark matter distribution (north-south). The circles represent the foreground galaxies of A370.

galaxies that are much bluer than nearby galaxies. The arcs that have been found in A370 may belong to this population.

Tyson's (1988) work suggests the intriguing possibility that the arcs found so far are merely the brightest and most distorted background sources and that there may conceivably be many other sources behind A370 that are more moderately distorted (Fort 1988). To understand what these sources might look like we have generated a synthetic background source plane populated randomly with faint galaxies distributed between redshifts of $z_S = 0.374$ (the lens redshift) and $z_S = 4.0$. The galaxies are assumed to have a constant comoving number density, and the background field has been adjusted to have 106 galaxies per square arcminute, corresponding to Tyson's counts at a limiting magnitude of $B_J = 27$. Luminosities are selected from a Schechter luminosity function and galaxies as faint as 0.01 $L_*$ are included, since these should be seen even out to $z_S = 4.0$ (Tyson 1988). The limiting isophotes that Tyson observes are a few magnitudes fainter than those of the arcs observed by F88. At this sensitivity, a galaxy will be detected well beyond its scale radius and so we represent the galaxies by circular disks of four scale radii.

Figure 5 shows the kind of distortions of faint background galaxies that we expect for a foreground cluster described by our best model of A370 ($\epsilon = 0.6$, $r_c = 10''$). In addition to the random background galaxies described above, we also include here the galaxies used in Figure 2 to produce the known arcs. For uniformity, we expand the sizes of these galaxies to four scale radii. Because of this, the corresponding images look significantly wider. A number of features are obvious in Figure 5:

1. The majority of images are elongated in the tangential direction with respect to the center of the cluster. The effect becomes particularly noticeable here because all the undistorted galaxies have been modeled to be circular (except the galaxy that produces A0). However, the magnitude of the distortion is so large in several cases that the effect should be noticeable even with a more realistic distribution of source galaxy shapes. This is, therefore, a direct test of the presence of dark matter and could be employed in any field of view that is suspected to contain a large amount of mass. A similar suggestion was made by Blandford *et al.* (1987) as a test of the suspected gravitational lens candidate 1146+111 B, C. As a by-product, the detection of tangential elongation in many faint images in a field would confirm that the faint blue galaxies that Tyson sees are not local dwarf galaxies but are indeed at large redshifts.

2. Further, by mere inspection of Figure 5 one can tell that the dark matter is significantly elongated in the north-south direction. For instance, elongated images are found out to the end of the field, over 60″ from the center of the cluster, in the north-south direction, but extend to less than 30″ in the east-west direction. Even the axis ratio of 2:1 probably can be guessed from a visual study of the map. A more detailed analysis, similar to that carried out in this paper, would provide a quantitative estimate of the ellipticity. We find this to be the most exciting implication of the present study, viz. that if one could detect a network of background sources, one would have a powerful tool to probe the *morphology* of dark matter in the field.

3. As a result of lensing, the galaxy images in Figure 5 are magnified (for example, compare the source and image planes). This allows better resolution of the images by up to a factor of 10 in fortunate cases. This might prove to be valuable in the study of very distant galaxies.

4. As a consequence of the magnification, the number density of the galaxy images is reduced near the cluster core. The effect is very pronounced in the simulation because we have taken a fixed cutoff in the galaxy luminosity function. In a more realistic situation, the effective cutoff will become fainter in the presence of lensing due to the so-called "amplification bias" (Turner, Ostriker, and Gott 1985). The exact effect on the number density then depends on the slope of the galaxy counts. If the slope of the cumulative counts is shallower than 0.8 per magnitude, then the number density will decrease in the presence of lensing. Tyson measures a slope of 0.45 for magnitudes brighter than $B_J \sim 27$. This slope could be probed to fainter magnitudes using foreground clusters as magnifying instruments.

Based on the above possibilities, we feel that deep imaging of rich clusters down to extremely faint magnitudes could be very profitable (Tyson 1988 has achieved 27 magnitudes per square arcsecond in J). Fort (1988) has also reached a similar conclusion, and we understand that J. A. Tyson and B. Fort and collaborators have already begun looking for these effects. One of us (S. A. Grossman, unpublished) has also been carrying out such observations. A complication is that the field of a rich cluster is not ideal for deep imaging of background objects because of the light from the cluster itself. To see how much interference this might cause, in Figure 5 we have plotted as open circles the positions of all the cluster galaxies in the field of A370 listed in BOW. It appears that there will be enough useful images in the spaces between foreground galaxies for many of the above effects to be seen.

We thank E. L. Turner for useful discussions. The comments of the referee, B. Fort, were invaluable and improved the paper appreciably. Comments by R. Wade were also helpful. This work was based on data retrieved from SIMBAD, data base of the Strasbourg, France, Astronomical Data Center, and was supported in part by the National Science Foundation under grant AST 88-14725.

## REFERENCES


Blandford, R. D., Phinney, E. S., and Narayan, R. 1987, *Ap. J.*, **313**, 28.
Butcher, H., Oemler, A., and Wells, D. C. 1983, *Ap. J. Suppl.*, **52**, 183 (BOW).
Coleman, G. D., Wu, C-C., and Weedman, D. W. 1980, *Ap. J. Suppl.*, **43**, 393.
Fall, S. M. 1981, in *The Structure and Evolution of Normal Galaxies*, ed. S. M. Fall and D. Lynden-Bell (Cambridge: Cambridge University Press), p. 1.
Fitchett, M. J. 1988, in *The Minnesota Lecture Series on Clusters of Galaxies and Large Scale Structure*, ed. J. M. Dickey (Astronomical Society of the Pacific), p. 143.
Fort, B. 1988, in *Astronomy, Cosmology, and Fundamental Physics—Third ESO/CERN Symposium, Bologna, May 16–20, 1988* (Dordrecht: Reidel).
Fort, B., Prieur, J. L., Mathez, G., Mellier, Y., and Soucail, G. 1988, *Astr. Ap.*, **200**, L17 (F88).
Giraud, E. 1988, *Ap. J. (Letters)*, **334**, L69.
Grossman, S. A., and Narayan, R. 1988, *Ap. J. (Letters)*, **324**, L37.
Hammer, F. 1987, in *High Redshift and Primeval Galaxies*, ed. J. Bergeron, D. Knuth, B. Rocca-Volmerange, and J. Tran Thanh Van (Paris: Editions Fontieres), p. 467.
Henry, J. P., and Lavery, R. J. 1987, *Ap. J.*, **323**, 473.
Lavery, R. J., and Henry, J. P. 1988, *Ap. J. (Letters)*, **329**, L21.
Lea, S. M., and Henry, J. P. 1988, *Ap. J.*, **332**, 81.
Lynds, R., and Petrosian, V. 1986, *Bull. AAS*, **18**, 1014.
———. 1989, *Ap. J.*, **336**, 1.
MacLaren, I., Ellis, R. S., and Couch, W. J. 1988, *M.N.R.A.S.*, **230**, 249 (MEC).
Mellier, Y., Soucail, G., Fort, B., and Mathez, G. 1988, *Astr. Ap.*, **199**, 13.
Mihalas, D., and Binney, J. 1981, *Galactic Astronomy* (San Francisco: Freeman).
Miller, J., and Goodrich, R. 1988, *Nature*, **331**, 685.
Narasimha, D., and Chitre, S. M. 1988, *Ap. J.*, **332**, 75.
Narayan, R., and Grossman, S. A. 1989, in *Gravitational Lenses*, ed. J. M. Moran, J. N. Hewitt, and K. Y. Lo (Berlin: Springer-Verlag), p. 31.
Paczyński, B. P. 1987, *Nature*, **325**, 572.
Pello-Descayre, R., Soucail, G., Sanahuja, B., Mathez, G., and Ojero, E. 1988, *Astr. Ap.*, **190**, L11.
Pence, W. D. 1976, *Ap. J.*, **203**, 39.
Sarazin, C. L. 1988, *X-Ray Emissions from Clusters of Galaxies* (Cambridge: Cambridge University Press).
Schechter, P. 1976, *Ap. J.*, **203**, 297.
Soucail, G., Fort, B., Mellier, Y., and Picat, J. P. 1987*a*, *Astr. Ap.*, **172**, L14.
Soucail, G., Mellier, Y., Fort, B., Hammer, F., and Mathez, G. 1987*b*, *Astr. Ap.*, **184**, L7.
Soucail, G., Mellier, Y., Fort, B., Mathez, G., and Cailloux, M. 1988, *Astr. Ap.*, **191**, L19.
Thompson, L. 1986, *Ap. J.*, **306**, 384.
Turner, E. L., Ostriker, J. P., and Gott, R. 1984, *Ap. J.*, **284**, 1.
Tyson, J. A. 1988, *A.J.*, **96**, 1.


*Note added in proof.*—Since the submission of this paper, we have become aware of three other studies of the arcs in Abell 370: I. Kovner (*Ap. J.*, **337**, 621 [1989]) and A. G. Bergmann, V. Petrosian, and R. Lynds (*Ap. J.*, submitted [1989]) have modeled the A0 arc, and F. Hammer and P. Rigaut (*Astr. Ap.*, in press [1989]) have modeled the A0, A5, and A6 arcs.

S. A. GROSSMAN and R. NARAYAN: Steward Observatory, University of Arizona, Tucson, AZ 85721